Author Manuscript

Author Manuscript

Author Manuscript

Author Manuscript

HHS Public Access

Author manuscript

Biochim Biophys Acta Gen Subj. Author manuscript; available in PMC 2021 September 02.

Published in final edited form as:

Biochim Biophys Acta Gen Subj. 2020 July ; 1864(7): 129548. doi:10.1016/j.bbagen.2020.129548.

Radiation Activates Myeloperoxidase (MPO) to Generate Active Chlorine Species (ACS) via a Dephosphorylation Mechanism - Inhibitory Effect of LGM2605

Om P. Mishra[a], **Anatoliy V. Popov**[b], **Ralph A. Pietrofesa**[a], **Wei-Ting Hwang**[c], **Mark Andrake**[d], **Eiko Nakamaru-Ogiso**[e], **Melpo Christofidou-Solomidou**[a]

[a]University of Pennsylvania Perelman School of Medicine, Department of Medicine, Pulmonary, Allergy, and Critical Care Division, Philadelphia, PA 19104

[b]Department of Radiology, Philadelphia, PA 19104

[c]Department of Biostatistics, Epidemiology, and Informatics, Philadelphia, PA 19104

[d]Molecular Modeling Facility, Fox Chase Cancer Center, Philadelphia, PA 19111

[e]Children's Hospital of Philadelphia, Department of Pediatrics, Philadelphia, PA 19104

Abstract

Background: Radiation exposure of tissues is associated with inflammatory cell influx. Myeloperoxidase (MPO) is an enzyme expressed in granulocytes, such as neutrophils (PMN) and macrophages, responsible for active chlorine species (ACS) generation. The present study aimed to: 1) determine whether exposure to γ-irradiation induces MPO-dependent ACS generation in murine PMN; 2) elucidate the mechanism of radiation-induced ACS generation; and 3) evaluate the effect of the synthetic lignan LGM2605, known for ACS scavenging properties.

Methods: MPO-dependent ACS generation was determined by using hypochlorite-specific 3 ´-(p-aminophenyl) fluorescein (APF) and a highly potent MPO inhibitor, 4-aminobenzoic acid hydrazide (ABAH), and confirmed in PMN derived from $MPO^{-/-}$ mice. Radiation-induced MPO activation was determined by EPR spectroscopy and computational analysis identified tyrosine, serine, and threonine residues near MPO's active site.

Address Correspondence to: Melpo Christofidou-Solomidou, Ph.D.: Department of Medicine, Pulmonary, Allergy, and Critical Care Division, University of Pennsylvania Perelman School of Medicine, 3450 Hamilton Walk, Stemmler Hall, Office Suite 227, Philadelphia, PA 19104. Phone: (215) 573-9917; Fax: (215) 746-0376, melpo@pennmedicine.upenn.edu.

AUTHOR STATEMENT

Om P. Mishra: Conceptualization, Methodology, Validation, Formal Analysis, Investigation, Data Curation, Writing – Original Draft, Visualization. **Anatoliy V. Popov:** Conceptualization, Methodology, Validation, Investigation, Writing – Original Draft. **Ralph A. Pietrofesa:** Methodology, Validation, Formal Analysis, Data Curation, Writing – Original Draft, Visualization. **Wei-Ting Hwang:** Methodology, Validation, Formal Analysis, Writing – Review & Editing, Visualization. **Mark Andrake:** Methodology, Validation, Formal Analysis, Investigation, Resources, Data Curation, Writing – Original Draft, Visualization. **Eiko Nakamaru-Ogiso:** Methodology, Validation, Formal Analysis, Investigation, Resources, Data Curation, Writing – Original Draft, Visualization. **Melpo Christofidou-Solomidou:** Conceptualization, Methodology, Validation, Formal Analysis, Resources, Data Curation, Writing – Original Draft, Visualization, Supervision, Funding Acquisition.

Publisher's Disclaimer: This is a PDF file of an unedited manuscript that has been accepted for publication. As a service to our customers we are providing this early version of the manuscript. The manuscript will undergo copyediting, typesetting, and review of the resulting proof before it is published in its final form. Please note that during the production process errors may be discovered which could affect the content, and all legal disclaimers that apply to the journal pertain.

Author Manuscript Author Manuscript Author Manuscript Author Manuscript

Results: γ-radiation increased MPO-dependent ACS generation dose-dependently in human MPO and in wild type murine PMN, but not in PMN from $MPO^{-/-}$ mice. LGM2605 decreased radiation-induced, MPO-dependent ACS. Protein tyrosine phosphatase (PTP) and protein serine/threonine phosphatase (PSTP) inhibitors decreased the radiation-induced increase in ACS. Peroxidase cycle results demonstrate that tyrosine phosphorylation blocks MPO Compound I formation by preventing catalysis on H_2O_2 in the active site of MPO. EPR data demonstrate that γ- radiation increased tyrosyl radical species formation in a dose-dependent manner.

Conclusions: We demonstrate that γ-radiation induces MPO-dependent generation of ACS, which is dependent, at least in part, by protein tyrosine and Ser/Thr dephosphorylation and is reduced by LGM2605. This study identified for the first time a novel protein dephosphorylation-dependent mechanism of radiation-induced MPO activation.

Keywords

Active Chlorine Species; Hypochlorite Ion; LGM2605; Myeloperoxidase; Radiation; Secoisolariciresinol Diglucoside

1. INTRODUCTION

It is well known that γ-radiation is capable of ionizing atoms and molecules. In biological systems or in solution, ionizing radiation generates hydroxyl radicals (•OH) [1–3], which are believed to be the source of ionizing radiation-induced damage to cellular components, including lipids, proteins, and DNA [4, 5]. However, these highly unstable hydroxyl radicals can be scavenged by Cl^- ions which are present at very high concentrations in physiological medium. This leads to the generation of active chlorine species (ACS) [6–9], among which relatively stable ClO^- was suggested as the radiation-derived toxicant [6]. HOCl (ClO^-), a potent oxidant, however, can also be produced by neutrophils containing activated myeloperoxidase (MPO), which catalyzes the reaction between physiologically present chloride ions and hydrogen peroxide (H_2O_2) [10]. Radiation-induced toxicity in normal tissues is an unwanted, but common, side effect of radiation exposure and an important limiting factor in radiotherapy [11]. Inflammatory responses to radiation are involved in tissue toxicity and MPO-containing neutrophils and macrophages are the key inflammatory cells recruited to exposed tissues [12]. However, the role of MPO activation by radiation in cells and the generation of ACS in response to radiation has never been studied. Indeed, the novel role of ACS in γ-radiation-induced cell damage has only been suggested in one publication [8]. In a recent study, we demonstrated the production of ACS in physiological solutions following γ-radiation and its role in radiation-induced DNA damage, and identified that LGM2605 scavenges ACS and protects DNA from radiation-induced damage [13].

MPO, a member of the hemeperoxidase-cyclooxygenase superfamily, is expressed in neutrophils, monocytes, and some tissue macrophages, and generates HOCl during inflammation and infection [14]. MPO catalyzes the reaction between Cl^- ions and H_2O_2 to generate a potent oxidant, HOCl [10, 14, 15]. MPO is an essential component in a number of pathological conditions, including cardiovascular, neurodegenerative, inflammatory and immune-mediated diseases [15–19]. The enzyme is involved in the innate immune response,

Author Manuscript Author Manuscript Author Manuscript Author Manuscript

as well as in microbial killing, by generating MPO-derived oxidants. Considering the involvement of MPO in a large number of human diseases, there is an urgent need for developing a highly selective MPO inhibitor that preserves MPO activity for host defense, but inhibits the excessive, persistent pathophysiological activation of MPO.

We have chemically synthesized two diastereomers of secoisolariciresinol diglucoside (SDG) [20], known as LGM2605, and shown to be equipotent in their antioxidant, free radical scavenging, and DNA protective properties [20, 21]. We showed that SDG protected DNA from γ-radiation-induced generation of ACS in physiological saline solutions [13]. Most importantly, we have also shown that LGM2605 inhibits MPO activity in inflammatory cells [22]. Due to these characteristics LGM2605 may be a useful agent to prevent radiation-induced, ACS-mediated cell and tissue damage.

In the present study, we: **1**) investigated the radiation-induced, MPO-dependent generation of ACS using a highly specific fluoroprobe, 3′-(p-aminophenyl) fluorescein (APF), for ACS in the presence of a highly potent MPO inhibitor, 4-aminobenzoic acid hydrazide (ABAH); **2**) elucidated the MPO-dependent mechanism of radiation-induced ACS generation using neutrophils from $MPO^{-/-}$ knockout mice; **3**) elucidated the dephosphorylation-mediated mechanism of radiation-induced, MPO-dependent ACS generation by using protein tyrosine phosphatase (PTP) and protein serine/threonine phosphatase (PSTP) inhibitors; **4**) determined the effect of LGM2605 (an ACS scavenger and MPO inhibitor) on radiation-induced, MPO-dependent generation of ACS; **5**) further elucidated the mechanism of radiation-induced MPO activation by determining the radiation-induced production of tyrosyl radical species that reflects generation of MPO intermediate Compound I using EPR spectroscopy; and **6**) highlighted several tyrosine/serine/threonine residues whose phosphorylation could modulate enzyme activity through a variety of mechanisms by examining MPO structures and analysis of the active site cavity.

2. MATERIALS AND METHODS

2. 1. Chemicals

ACS indicator probe APF was purchased from ThermoFisher Scientific (Carlsbad, CA). Sodium hypochlorite, sodium orthovanadate (SOV, PTP inhibitor), hMPO from human leukocytes, and MPO fluorometric activity assay kit were purchased from Sigma-Aldrich (St. Louis, MO). H_2O_2 was purchased from Fisher Scientific (Hampton, NH). HOCl concentration was documented spectrophotometrically in 10 mM NaOH at pH 12 using the molar extinction coefficient at 292 nm ($\varepsilon_{292\,=}$ 350 M^{-1} cm^{-1}). Dulbecco's phosphate buffered saline (DPBS 1X, 21–031-CV) without calcium and magnesium was purchased from Mediatech Inc. (Manassas, VA). Halt phosphatase inhibitor cocktail (PTP + PSTP inhibitors) was purchased from ThermoFisher Scientific (Waltham, MA). Okadaic acid (PSTP inhibitor) was purchased from MilliporeSigma (Burlington, MA). Amplex Red hydrogen peroxide/peroxidase assay kit was purchased from ThermoFisher Scientific (Carlsbad, CA). Synthetic SDG (LGM2605) was purchased from Chemveda Life Sciences Pvt. Ltd. (Hyderabad, India) based on procedure developed by our group. Structures of SDG and protein phosphatase inhibitors are shown in Supplemental Figure 1.

Author Manuscript Author Manuscript Author Manuscript Author Manuscript

2.2. Derivation of Elicited Murine Neutrophils

To obtain murine neutrophils, wild type C57Bl/6 mice (Charles River Laboratories, Wilmington, MA) and $MPO^{-/-}$ knockout mice (B6.129X1-*Mpo* $^{tm1L\ us}$/J; Jackson Laboratory, Bar Harbor, ME; strain of origin, 129X1/SvJ) were injected intraperitoneally with 2 ml of thioglycollate medium (Becton Dickinson, Franklin Lakes, NJ). After 6 hours, belly lavage was performed with intraperitoneal instillation of 10 ml sterile 1X PBS containing Ca^{2+} and Mg^{2+} through a 20-gauge angiocatheter (BD Pharmingen, San Diego, CA). After the peritoneal cavity of the mouse was gently massaged, approximately 10 ml of lavage fluid was removed through the 20-gauge angiocatheter. A small aliquot of lavage fluid was immediately spun on a Shandon Cytospin-3 cell preparation system (Thermo Electron, Waltham, MA) at 1500 revolutions per minute (rpm) for 10 minutes and stained with a standard Hemacolor stain set protocol from MilliporeSigma (Burlington, MA) to confirm the presence of neutrophils in the lavage fluid. The remaining lavage fluid was centrifuged at 1200 rpm for 10 minutes and the pelleted cells were then suspended in DPBS, DPBS + SOV, DPBS + PTP + PSTP inhibitors, and DPBS + okadaic acid. ACS generation and murine MPO (mMPO) activity were determined as described below.

2.3. γ-Radiation-Induced Generation of MPO-Dependent HOCl and the Scavenging Effect of SDG (LGM2605) using hMPO and Murine Neutrophils

Myeloperoxidase from human (hMPO) or murine polymorphonuclear cells from $MPO^{+/+}$ or $^{-/-}$ mice (10,000 cells/200 μl medium/well) in PBS, pH 7.4 (DPBS) with APF were exposed to doses of γ-radiation ranging from 0 to 25 Gy using a Mark 1 cesium (^{137}Cs) irradiator (J.L. Shepherd, San Fernando, CA) at a dose rate of 1.7 Gy/min in room air (21% O_2) at 0 °C. To determine MPO-dependent generation of ACS, experiments were performed in presence of a highly potent inhibitor of MPO, ABAH (100 μM). Phosphorylation dependence was determined in the presence of protein tyrosine phosphatase as well as Ser/Thr phosphatase inhibitors. The effect of LGM2605 was determined at various concentrations. Following radiation, the fluorescence of fluorescein, formed under HOCl-mediated cleavage of APF, was determined immediately. The fluorescence intensity for the APF probes (10 μM) was measured at excitation/emission wavelengths of 490 nm/515 nm in a Molecular Devices Spectramax i3 (Molecular Devices, Sunnyvale, CA). Prior to radiation exposure and ACS measurements, cells were suspended in a medium containing PBS or PBS with inhibitors.

2.4. Myeloperoxidase Activity

hMPO from human leukocytes purchased from MilliporeSigma (Burlington, MA) was used to determine the effect of LGM2605 on MPO activity. The MPO activity was assayed, using the myeloperoxidase fluorometric activity kit (MilliporeSigma, Burlington, MA), as described by the manufacturer by determining the increase in fluorescence intensity of APF at 485 nm excitation/ 525 nm emission wavelengths at room temperature. MPO-dependent increase was determined in the presence of MPO inhibitor, ABAH (100 μM). The activity was determined in presence of various concentrations of LGM2605 between 0–100 μM.

Author Manuscript Author Manuscript Author Manuscript Author Manuscript

2.5. Myeloperoxidase Activity of Elicited Neutrophils from Wild type and MPO$^{-/-}$ Mice

The MPO activity in murine neutrophils (10,000 cells/200 μl medium/well) was assayed using the myeloperoxidase fluorometric activity kit (MilliporeSigma, Burlington, MA), as described by the manufacturer. Supernatant aliquots (50 μl) were placed in 96-well black clear bottom plates and mixed with 50 μl solution containing (substrate and probe) H_2O_2 and APF. The final concentrations of H_2O_2 and APF were 50 μM and 25 μM, respectively. MPO-dependence was determined in the presence of the MPO inhibitor, ABAH (100μM). To determine the dependence of MPO activity on protein phosphorylation, experiments were performed in the presence of inhibitors of protein tyrosine phosphatase as well as Ser/Thr phosphatases. MPO activity was continuously monitored by determining the increase in fluorescence at excitation/emission wavelengths of 485 nm/525 nm in a Molecular Devices Spectramax i3 (Molecular Devices, Sunnyvale, CA).

2.6. Determination of Myeloperoxidase Activity (Peroxidase Cycle)

hMPO purified from human leukocytes (MilliporeSigma, Burlington, MA) was used to determine the effect of PTP and PSTP inhibitors on MPO activity. The activity was determined using the Amplex Red hydrogen peroxide/peroxidase assay kit (ThermoFisher Scientific, Carlsbad, CA) that determines H_2O_2 concentration based on the oxidation of Amplex Red to the fluorescent product resorufin. The excitation and fluorescence emission wavelengths were 530 nm and 590 nm, respectively. The assay was performed in the absence of chloride with varying concentrations of H_2O_2 in the presence or absence of PTP inhibitor (SOV, 0.25 mM) and PSTP inhibitor (okadaic acid, 100 nM). H_2O_2 was added last to initiate the reaction. Michaelis-Menten enzyme kinetics were determined using GraphPad Prism version 6.00 for Windows, GraphPad Software, La Jolla, CA, USA (www.graphpad.com). The maximum enzyme velocity (V_{max}) and Michaelis-Menten constant (K_m) were determined using the model $Y = V_{max}*X / (K_m + X)$, where X represents the varying concentrations of H_2O_2.

2.7. EPR Spectroscopy of γ-Irradiated MPO

EPR samples were freshly prepared. Native freeze-dried hMPO enzyme from human leukocytes (MilliporeSigma, Burlington, MA) was dissolved in 50 mM sodium phosphate buffer pH 7.4 to 1 mg/ml (12.34 μM). 230 μl of enzyme solution was transferred into five different tubes for five different conditions: (a) non-irradiated (0 Gy); (b) irradiated (10 Gy); (c) irradiated (25 Gy); (d) non-irradiated + H_2O_2 (0 Gy); (e) irradiated + H_2O_2 (25 Gy). Samples were transferred into EPR tubes and then exposed to 0 Gy, 10 Gy, or 25 Gy. The samples were frozen at 10 seconds after radiation in pre-cooled ethanol dry ice and stored in liquid nitrogen. We used a special mixer for mixing samples quickly in EPR tubes, which was previously described [23]. EPR spectra were recorded by a Bruker Elexsys E500 spectrometer at X-band (9.4 GHz) using an Oxford Instrument (Abingdon, United Kingdom) ESR900 helium flow cryostat.

2.8. Structural Analysis of Candidate Serines, Threonines, and Tyrosines

Cavity analysis of the known structure of mature MPO (PDB code 1DNW) was performed using the methods of [24], using the CAVITY module which outputs all potential ligand-

Author Manuscript Author Manuscript Author Manuscript Author Manuscript

binding sites on the protein surfaces and the druggability of all detected cavities. This was done without including existing ligands in 1DNW and enumerated the residues contributing atoms to the contiguous surface of protein cavities. The calculation of the cavity volumes was done in Chimera, after building a surface for the identified residues, followed by the "measure volume" command. The per residue normalized solvent excluded surface area (SESA) for each serine, threonine and tyrosine in the major cavity was calculated in Chimera using the method of normalization described in [25]. Analyses of hydrogen bonds, solvent accessible surface area, as well as figure and movie preparation were performed with Chimera (UCSF) [26].

2.9. Statistical Analysis of the Data

All samples were evaluated in triplicate and the data obtained are presented as the mean ± the standard error of the mean (SEM). Data obtained from experiments evaluating various doses of radiation exposure and enzyme inhibition were analyzed using two-way analysis of variance (ANOVA) to test for the main effects of radiation dose and treatment type, along with the interaction between these variables, on experimental outcomes. If the overall F-test was statistically significant, post-hoc tests (Tukey's honest significance tests) were conducted analyzing significant differences among treatment groups; both between and within each respective radiation dose level. All enzyme kinetic data were analyzed using two-way repeated measures ANOVA to test for the main effects of time and treatment, along with the interaction between these variables, on experimental outcomes, followed by Tukey's honest significance tests if the overall F-test was statistically significant.

One-way analysis of variance (ANOVA) was used to compare various types and doses of MPO inhibitors, followed by post-hoc comparisons (Tukey's honest significance tests) if the overall F-test was statistically significant. All analyses were performed using GraphPad Prism version 6.00 for Windows, GraphPad Software, La Jolla, CA, USA (www.graphpad.com). All tests were two-sided and statistically significant differences were determined at p-value < 0.05. Asterisks shown in figures indicate statistically significant differences between treatment groups across different levels of a particular variable (* : $p < 0.05$, ** : $p < 0.01$, *** : $p < 0.001$, and **** : $p < 0.0001$), while # shown in figures indicate statistically significant differences between treatment groups within different levels of a particular variable (# : $p < 0.05$, ## : $p < 0.01$, ### : $p < 0.005$, and #### : $p < 0.001$).

3. RESULTS

3.1. Radiation Induces MPO-dependent Generation of ACS

To elucidate that γ-irradiation induces MPO-dependent ACS, we exposed 1, 2, and 20 ng/well (in 96-well black clear bottom plates) hMPO in DPBS to 0, 5, 15, and 25 Gy radiation exposure and the generation of ACS was determined by the cleavage of APF. Results in Figure 1A show that there is a radiation dose-dependent increase in fluorescein fluorescence and the radiation-induced increase in ACS is significantly higher at all the radiation doses in the presence of MPO, indicating MPO-dependent increase in ACS by radiation (p<0.0001). Figure 1B shows that the radiation-induced increase in fluorescein fluorescence is significantly decreased in the presence of MPO inhibitor ABAH (100 μM) (p<0.0001).

Author Manuscript Author Manuscript Author Manuscript Author Manuscript

These results further demonstrate that the radiation-induced increase in ACS generation is MPO-dependent. Figure 1C shows that the radiation-induced MPO-dependent ACS generation, as a function of radiation dose, is curvilinear; the enzyme is probably getting partially inactivated at higher doses of radiation. The MPO-independent ACS generation was 5-times slower compared to the MPO-dependent ACS generation, but it was linear. These results demonstrate that γ-irradiation induces MPO-dependent generation of ACS and also confirms our previous observation of radiation-induced MPO-independent component in physiological solutions as well [13]. These results demonstrate that γ-irradiation generates ACS by both MPO-dependent, as well as MPO-independent, pathways.

3.2. LGM2605 Inhibits γ-Radiation-induced, MPO-dependent Generation of ACS in Isolated hMPO

In our previous study, we found that LGM2605 inhibits MPO activity [27]. To investigate whether LGM2605 inhibits radiation-induced, MPO-dependent ACS, hMPO was exposed to radiation along with LGM2605, and the ACS generation was determined. LGM2605 (10, 25, 50, and 100 μM) was added before exposure to radiation. Figure 2A shows that the increase in MPO-dependent ACS generation at various doses of radiation is significantly inhibited by LGM2605, dose-dependently ($p<0.01$). Importantly, the inhibition by LGM2605 is comparable to the inhibition by a highly selective MPO inhibitor, ABAH. Figure 2B shows that LGM2605 significantly decreased radiation-induced ACS generation in a dose-dependent manner ($p<0.05$). These results demonstrate that LGM2605 inhibits γ radiation-induced generation of ACS.

3.3. Radiation-induced, MPO-dependent Generation of ACS in Neutrophils Isolated from Wild Type and MPO Knockout Mice

To elucidate that γ-irradiation induces MPO-dependent generation of ACS in cells, we isolated elicited neutrophils from WT and $MPO^{-/-}$ mice. Cells were then exposed to γ-radiation at 0 Gy and 25 Gy in the presence of APF, and the generation of ACS was determined. ACS generation, as well as MPO activity, were determined in the absence, as well as in the presence, of the MPO inhibitor ABAH (100μM). Results in Figure 3A show that there is a significant increase in fluorescein fluorescence at 25 Gy as compared to 0 Gy and that the radiation-induced increase is significantly lower in the $MPO^{-/-}$ neutrophils as compared to WT ($p<0.0001$). A much lower MPO activity in neutrophils from $MPO^{-/-}$ mice, as compared to WT mice, was confirmed and the results are presented in Figure 3B ($p<0.0001$). These results clearly demonstrate that the radiation-induced generation of ACS in mouse neutrophils is MPO-dependent.

3.4. LGM2605 Inhibits γ-Radiation-induced, MPO-dependent Generation of ACS in Murine Neutrophils

Next, we investigated whether LGM2605 inhibits radiation-induced MPO-dependent ACS generation in murine neutrophils. Elicited neutrophils isolated from WT mice were exposed to radiation (0 Gy or 25 Gy) with or without LGM2605, and ACS generation was determined. LGM2605 was added prior to radiation exposure. MPO dependence was determined in the presence of MPO inhibitor, ABAH (100 μM). Figure 4A shows that LGM2605 dose-dependently decreased radiation-induced ACS ($p<0.0001$). Figures 4B

Author Manuscript Author Manuscript Author Manuscript Author Manuscript

shows the LGM2605 dose-dependent decrease of ACS generation as percent of control (in the absence of LGM2605) ($p<0.0001$). These results demonstrate that LGM2605 inhibits γ-radiation-induced generation of ACS in murine neutrophils.

3.5. γ-Radiation-Induced, MPO-Dependent Generation of ACS in Murine Neutrophils is Mediated by Protein Dephosphorylation

To elucidate that the γ radiation-induced MPO-dependent generation of ACS is mediated by protein dephosphorylation, we isolated elicited murine neutrophils, as a source of MPO, in DPBS, and DPBS with PTP inhibitor (SOV), DPBS with PSTP inhibitor (okadaic acid) and PTP+PSTP phosphatase inhibitors (Halt phosphatase inhibitors). The cells were exposed to radiation (0 Gy or 25 Gy), and ACS generation was determined. The protein phosphatase inhibitors were present before irradiation. The results show that the radiation-induced ACS generation is significantly decreased in the presence of protein phosphatase inhibitors for PTP (Figure 5B), PSTP (Figure 5C) and PTP+PSTP (Figure 5A) ($p<0.0001$). This indicates that phosphorylation at either Tyr or Ser/Thr residues can decrease ACS generation. The inhibition was cumulative and larger in the presence of both PTP and PSTP inhibitors. Figures 5A, 5B, and 5C also show MPO-dependent ACS generation at 0 Gy. Figures 5D, 5E and 5F show the data as percent of control (at 25 Gy) in absence of inhibitors. In presence of inhibitors for both PTP and PSTP, there is up to a 60% decrease in radiation-induced ACS generation. These results demonstrate that protein phosphorylation status affects radiation-induced, MPO-dependent ACS generation in murine neutrophils, and phosphorylation of MPO seems to inhibit the MPO activity, which is not known previously. These results demonstrate that radiation-induced, MPO-dependent ACS generation in murine neutrophils is mediated by protein dephosphorylation. This is a unique and novel observation that has not been reported elsewhere.

3.6. Role of Protein Dephosphorylation in MPO Activity of Murine Neutrophils

To elucidate the role of protein dephosphorylation in mMPO activity in murine PMN, cells were harvested and suspended in DPBS, DPBS + PTP inhibitor SOV, DPBS + PSTP inhibitor (okadaic acid) and in DPBS + PTP and PSTP inhibitors, and mMPO activity was determined. Results **s**how a statistically significant inhibition of mMPO activity in presence of protein phosphatase inhibitors, indicating that protein phosphorylation results in decreased mMPO activity (Figure 6A) ($p<0.05$). Figure 6B shows the results as percent of control activity (without inhibitors) in presence of protein phosphatase inhibitors. Data with the MPO inhibitor ABAH are shown in Supplemental Figure 2. These results demonstrate that mMPO activity in murine neutrophils is enhanced by protein dephosphorylation. Dephosphorylation dependence of MPO activity in the presence of protein tyrosine phosphatase is shown in Supplemental Figure 3. The results show that MPO activity was significantly increased by PTP treatment ($p<0.0001$). The initial slope increased by 60% following PTP treatment indicating that MPO activity is dephosphorylation-dependent.

3.7. Role of Protein Dephosphorylation in Peroxidase Cycle of MPO in Murine Neutrophils

To further elucidate the role of protein tyrosine dephosphorylation or protein serine/threonine dephosphorylation specifically on the peroxidase catalytic activity of MPO, we

Author Manuscript Author Manuscript Author Manuscript Author Manuscript

performed peroxidase cycle activity in absence of chloride (to prevent chlorination cycle) in the medium. The activity was performed in PB, PB + SOV and PB + okadaic acid. Figure 7 shows the peroxidase cycle activity under control and with inhibitors. SOV (PTP inhibitor) completely blocks the H_2O_2-dependent increase in enzyme activity at varying concentrations of H_2O_2 (Figure 7B and 7D). In contrast, okadaic acid (PSTP inhibitor) appears to activate the peroxidase cycle (Figures 7C and 7D). Data with 0 μM H_2O_2 are shown in Supplemental Figure 4. The results show a 98.6% decrease in Vmax in presence of SOV (Vmax = 1.02 ± 0.15 × 10^6 RFU without SOV compared to 1.52 ±1.77 × 10^4 RFU with SOV) (Figure 7D). There was no activity even under high concentrations of H_2O_2, indicating that SOV completely blocks H_2O_2 accessing to the active site of MPO. In presence of okadaic acid, the Vmax values were similar (Vmax = 1.18 ±0.10 × 10^6 RFU with okadaic acid as compared to Vmax = 1.02 ± 0.15 × 10^6 RFU in control). The Km values were lower in the presence of okadaic acid (Km = 0.80 ± 0.57 μM H_2O_2 with okadaic acid as compared to Km = 4.63 ± 2.38 μM H_2O_2 in control). The results indicate that dephosphorylation of Ser/Thr may not be required for catalytic activity of the peroxidase cycle of MPO with H_2O_2 as a substrate. These results indicate that protein tyrosine phosphorylation more specifically interferes with the MPO catalytic activity using H_2O_2 as a substrate.

3.8. EPR Spectroscopy of γ-Irradiated hMPO

Since the peroxidase cycle of MPO involves tyrosine radical formation, we determined generation of tyrosine radical species in hMPO using EPR Spectroscopy. MPO solution was divided into five groups: (a) non-irradiated (0 Gy); (b) irradiated (10 Gy); (c) irradiated (25 Gy); (d) non-irradiated + H_2O_2 (0 Gy); (e) irradiated + H_2O_2 (25 Gy). Results presented in Figures 8A and 8B show the EPR spectra of hMPO under the above five conditions. The results show an increase in tyrosyl radical formation at 10 and 25 Gy exposure group. There is no tyrosyl spectra at 0 Gy. Presence of H_2O_2 did not affect the results. These results identify radiation-induced generation of tyrosyl radicals and confirm their radiation dose-dependent generation. The tyrosyl radical generation by radiation may modify the MPO protein by intermolecular and intramolecular bi-tyrosine formation, and result in altered MPO activity post radiation exposure. These results demonstrate radiation-induced dose-dependent activation of hMPO, a novel finding that has not been reported elsewhere.

4. DISCUSSION

In a recent study, we have demonstrated that γ-irradiation produces ACS in physiological solutions [13]. ACS were scavenged by SDG, the main lignan in whole grain flaxseed. Considering the extensive use of radiation therapy in >50% lung cancer patients, the current study was designed to identify if radiation exposure induces MPO-dependent generation of ACS in inflammatory cells. We have also examined the effect of synthetic SDG (LGM2605) on radiation-induced, MPO-dependent generation of ACS. The important findings of this study are that: **1**) γ-irradiation enhanced MPO-dependent generation of ACS by 5 times in hMPO and murine neutrophils; **2**) radiation-induced, MPO-dependence of ACS was confirmed using MPO knockout mice; **3**) SDG (LGM2605) decreased the radiation-induced, MPO-dependent generation of ACS in hMPO and murine neutrophils; **4**) radiation-induced ACS generation is protein Tyr and Ser/Thr dephosphorylation-mediated; **5**) MPO activity

Author Manuscript Author Manuscript Author Manuscript Author Manuscript

was Tyr and Ser/Thr dephosphorylation-dependent in non-irradiated cells; and **6**) EPR studies identified a radiation induced generation of tyrosyl radical species in MPO and the generation was radiation-dose dependent.

Considering the extensive use of radiation therapy in lung cancer patients worldwide, the significance of radiation-induced, MPO-dependent generation of ACS and ACS-induced damage to cellular components, including DNA, would be a novel and predominant mechanism of radiation damage. In addition, the results demonstrate that LGM2605 prevented the radiation-induced, MPO-dependent ACS generation. Since LGM2605 decreases radiation-induced, MPO-dependent generation of ACS as shown in the present study, the potential role of LGM2605 as a therapeutic agent appears highly significant for preventing radiation damage in cancer patients undergoing radiation therapy.

We have previously demonstrated the antioxidant and radioprotective characteristics of the synthetic SDGs (*R,R* and *S,S* diastereomers) by assessing their potential for scavenging free radicals and preventing γ-radiation-induced damage to plasmid DNA (pBR322) and calf thymus DNA [20, 21], as well as in a mouse model of thoracic radiation damage using the whole grain dietary flaxseed [28–31]. Furthermore, we have shown that SDG scavenges radiation-induced ACS generated in MPO-independent and MPO-dependent mechanisms.

MPO generates HOCl that kills invading microorganisms by oxidative damage [32]. HOCl modifies adenine nucleotides resulting in formation of chloramines that appears to be a major mechanism of neutrophil-mediated toxicity [33–35]. An increased and persistent activation of MPO-H_2O_2-Cl^- system may lead to tissue damage by modifying lipids, nucleobases of DNA and proteins by chlorination, nitration, and oxidative reactions. MPO is expressed in neutrophils, monocytes, and tissue macrophages and is a key factor in cardiovascular, neurodegenerative, inflammatory, and immune-mediated diseases [36–39].

Our finding is that radiation-induced, MPO-dependent ACS generation is affected by the phosphorylation status of MPO, and both protein tyrosine or protein Ser/Thr phosphatase inhibitors attenuate the MPO's radiation-dependent ACS generation ability. Dependence of MPO's activity on protein tyrosine or protein Ser/Thr phosphorylation has not been mentioned before. In addition, radiation-induced, MPO-dependent ACS generation has not been shown before to be mediated, at least in part, by protein tyrosine and protein Ser/Thr phosphorylation. Considering the role of MPO in cell death and in innate, as well as acquired, immunity, our findings are highly significant.

Radiation-induced ACS generation was significantly decreased by PTP inhibitor in murine neutrophils indicating the dependence of ACS generation on protein tyrosine dephosphorylation. These results indicate that protein tyrosine and serine/threonine dephosphorylation yields higher (full) MPO activity and radiation-induced increased ACS generation. Considering the structure of the MPO molecule, there are 11 tyrosines: 1 in the small subunit whereas 10 in the large subunit. There are two pairs of tyrosine and serine residues (470 Tyr, 472 Ser, 473 Tyr; 714 Ser, 715 Tyr), where Tyr and Ser residues are adjacent or in close vicinity [40]. We propose that tyrosine and serine phosphorylation/dephosphorylation can regulate MPO catalytic activity and radiation-induced, MPO-

Author Manuscript Author Manuscript Author Manuscript Author Manuscript

dependent ACS generation. Most probably, the tyrosine phosphorylation of MPO-mediates radiation-induced ACS generation and serine phosphorylation on a neighboring Ser interferes with tyrosine phosphorylation. This may be due to a steric hindrance created by the bulky phosphate groups and thereby affecting radiation-induced ACS generation or vice versa. Results presented here on the effect of protein tyrosine and protein serine/threonine phosphatase inhibitors indicate that protein tyrosine phosphorylation blocks the access of H_2O_2 to the active site of MPO, whereas serine phosphorylation activates the cycle, further indicating the role of phosphorylation in regulation of MPO activity. Serine phosphorylation may be inhibitory to the chlorination cycle, as okadaic acid inhibits the overall reaction of HOCl generation (Figure 6).

Using EPR spectroscopy, we have identified radiation-induced generation of tyrosyl radical species in MPO. The radiation-induced increase in tyrosyl radical formation was dose-dependent. The presence or absence of H_2O_2 did not affect tyrosyl radical formation. In MPO-catalyzed reaction, MPO Fe(III) is converted by H_2O_2 to MPO-Fe (IV)=O (the Compound I intermediate) (Figure 9), which is reduced by two-electron reduction by Cl^- to generate HOCl in the chlorination cycle. As in the present study, the experiment was performed in the absence of Cl^-, the MPO-Fe (IV)=O (Compound I) is reduced by tyrosine (a molecule that competes for the same site as Cl^-) in a single electron reduction to compound II and then another one-electron reduction to native MPO-Fe (III). The rate constant for tyrosine oxidation for the MPO Compound I reaction is comparable to that of its reaction with Cl^- [41–43]. The generation of tyrosyl radical in our experiments reflects the generation of Compound I, MPO-Fe (IV)=O, during radiation. EPR spectrum of a spin-trapped radical in MPO compound I generated in presence of H_2O_2 has been reported and suggested that it might be a Tyr radical [44].

The radiation-induced increase in the generation of tyrosyl radicals in MPO might result in intermolecular, as well as intramolecular, di-tyrosine formation [42, 45] and subsequently affect MPO activity. In addition, radiation generated tyrosyl radicals may lead to the formation of tyrosine derivatives, including 3-chlorotyrosine and 3-nitrotyrosine, and lipid radicals [15, 46, 47]. Furthermore, in comparison to tyrosine-OH that reduces Compound I, phosphorylated tyrosine may not participate in reduction of Compound I. Therefore, tyrosine phosphorylation of the protein would result in decreased levels of tyrosyl radical formation. Our proposed mechanism of radiation-induced, MPO-dependent generation of HOCl and of tyrosyl radical, and the role of tyrosine dephosphorylation is presented in Figure 9. Figure 9 shows the proposed mechanism of radiation-induced, MPO-dependent ACS generation without protein tyrosine phosphatase (PTP) inhibitor (Figure 9A) and with PTP inhibitor (Figure 9B). In Figure 9A, steps 1, 3 and 5 show the **peroxidase cycle** of MPO reaction; Step 2 shows the **chlorination cycle** of MPO reaction. Step 1 shows the two-electron oxidation of native MPO-Fe (III) to compound I (MPO-Fe(IV)=O Por.+ (also suggested as to be MPO-Tyrosyl radical, MPO-Tyr). Steps 3 and 4 (in absence of any reducing agent) show generation of tyrosyl radical production, while generating Compound II intermediate, using intermolecular, as well as intramolecular, MPO-tyrosine residues. These two are one-electron reduction of Compound I to Compound II and subsequently to native MPO-Fe(III). Step 2 shows two-electron oxidation of Cl^- that results in production of HOCl. In Figure 9B,

Author Manuscript Author Manuscript Author Manuscript Author Manuscript

steps 5 and 6 (identical to Step 1 and 2 in Figure 9A) do not proceed in the presence of PTP inhibitor. Step 7 shows that PTP inhibitor blocks dephosphorylation of phosphorylated MPO to non-phosphorylated native MPO, thus resulting in increased tyrosine-phosphorylated MPO. Figures 9C and 9D show MPO-Tyr-OH and MPO-Tyr-phosphorylated structures.

Protein tyrosine phosphorylation is a critical event that controls a number of oncogenic signaling pathways of cell proliferation, apoptosis, migration and invasion [48, 49]. In fact, several PTPs are tumor suppressors [50–52]. The first proteotypic member of the PTP family is PTP1B whose crystal structure provided the basis for understanding the mechanism of action of PTPs [53, 54]. PTPs and dual specificity phosphatases (DSPs) share the same mechanism of action and have a conserved catalytic motif $HC(X)_5R$ [48, 55]. The catalytic cysteine residue sits at the bottom of the catalytic cleft. In addition, there is an aspartate residue essential for the two-step mechanism of action of PTPs. Mutations at these residues (cysteine to serine, or aspartate to alanine) abolished PTP activity. Radiation-induced, MPO-dependent generated HOCl can interact with the cysteine residue [56] of the protein phosphatase and inhibit the first step of the dephosphorylation reaction resulting in increased phosphorylation of tyrosine residue in MPO. Thus, HOCl can downregulate MPO activity by phosphorylation of tyrosine and serine residues. Results presented here in the presence of protein phosphatase inhibitors support this idea. In present studies, the presence of PTP and PSTP inhibitors, even at highest concentrations, only partially inhibited the radiation-induced ACS generation indicating that MPO dephosphorylation is, in part, a mechanism of radiation-induced MPO activation.

In our studies, radiation-induced HOCl could modify the active site cysteine residue of PTP leading to inactivation of the enzyme, which, in turn, would increase tyrosine phosphorylation of MPO. Redox-based regulation of PTPs has been established. In the presence of PTP inhibitor, the increased tyrosine phosphorylation is associated with a decrease in radiation-induced ACS generation. These results demonstrate that radiation-induced ACS generation is tyrosine phosphorylation-mediated. The opposing effect of PTP and PSTP inhibitors on H_2O_2 active site of MPO indicates that tyrosine and serine phosphorylation may modulate and regulate MPO activity. A mechanism of PTP regulation by PSTP-specific phosphorylation is well known. This covalent modification regulates PTP in a negative manner as in case of PTP-PEST when phosphorylated on Ser 39/Ser434 by protein kinase A or protein kinase C. Of course, the effect of tyrosine or serine phosphorylation/dephosphorylation on function of MPO will be residue and site specific.

To understand which specific residues are located in a position able to modulate catalysis of hMPO, we conducted a structural analysis of candidate serines, threonines, and tyrosines. In the portion of the protein of known structure (PDB code 1DNW) there are 29 threonines, 30 serines, and 15 tyrosines for a total of 74 sites capable of phosphorylation. Of these 74 residues, only 11 are known to be phosphorylated by phospho-proteomics studies (see Table 1 and Supplemental Table 1) [57]. A careful mapping of these candidate residues on the known MPO structure could highlight the potential mechanisms where phosphorylation might inhibit enzyme activity.

Author Manuscript Author Manuscript Author Manuscript Author Manuscript

Cavity analysis [24] of the MPO structure found in PDB accession code 1DNW reveals only one major cavity of 8,567Å^3, the one containing the active site heme. All other cavities are below a volume of 2700 Å^3, and deemed to have no appreciable ligand/drug binding capacity. It is most probable that all substrate entry and product exit occur on the same distal side of the heme through this main cavity. The 95 residues that line this cavity are shown in Supplemental Table 2. Among these 95 residues are 4 serines (149,179,240,241), 5 threonines (100,117,238,329,337) and 2 tyrosines (296,334), which are at the base of the cavity on the proximal side (see Figures 10A and 10B). All but two (T329 and S337) of the serines/threonines are located on the distal side of the heme. When examining the location of these residues within this cavity, it is possible to envision at least three mechanisms whereby phosphorylation could inhibit the activity of MPO.

The first mechanism could be that phosphorylation introduces a steric hindrance that restricts substrate access to the active site heme. The residue whose phosphorylation would be the most likely to restrict substrate access to the distal heme cavity is T238 (see Figures 10B and 10C). A second mechanism could involve disruption of heme position in relation to active site residues required for catalytic activity, such as H95 and H336. T238 along with two nearby serines 240 and 241 could be phosphorylated in a cooperative manner just after translation and prior to MPO maturation and heme addition. Phosphorylation at 240 or 241 would be expected to adversely affect the exact positioning of adjacent E242/C243 residues that are subsequently covalently linked to the heme (see Figure 10B). Any alteration in C243 position would phenocopy mutations like C243M that lead to a decrease in oxidation of chloride and bromide [58]. To prevent such inactivation, the action of phosphatases might be required. There is precedent for PTP1B regulation of a precursor protein by dephosphorylation during biosynthesis in the endoplasmic reticulum [59]. Even though T117 is near the top of the cavity opening, its phosphorylation is not likely to sterically hinder substrate access to the heme cavity (see Figure 10C).

A third mechanism of inhibition could occur through phosphorylation of the two tyrosines (296,334) on the proximal side of the heme at the base of the cavity (see Figure 10A), which are known to be hydrogen bonded to each other. Phosphorylation of either tyrosine would alter Y334 position which is on the opposing face of the same helix that anchors the catalytic H336. The exact position of H336 and its interactions with the heme iron are central to the MPO catalytic mechanism. H336 participates with two other residues (N421, R333) in a proximal side triad [60]. It is already known that disruption of this triad, by mutation of N421 to Asp decreased the rate at which H_2O_2 reacted to form Compound I, eliminated oxidation of chloride, and markedly decreased oxidation of bromide and tyrosine. Phosphorylation of the either tyrosine on the opposing side of the H336 helix would be expected to have the same negative effect on MPO catalytic activity. Also the role of these two tyrosine residues in radiation induced increase of ACS formation and peroxidase activity could involve radiation enhanced tyrosyl radical formation of di-tyrosine cross-links. This would be consistent with their close proximity to each other, and the EPR result showing radiation induced tyrosyl radical formation in Figure 9.

In summary, we have demonstrated that γ-radiation induces MPO-dependent generation of ACS in hMPO and murine neutrophils. Radiation-induced, MPO-dependent ACS

Author Manuscript Author Manuscript Author Manuscript Author Manuscript

generation was confirmed using neutrophils from MPO knockout mice. (LGM2605) decreased the radiation-induced, MPO-dependent generation of ACS. The radiation-induced, MPO-mediated ACS generation in part was protein Tyr and Ser/Thr dephosphorylation-mediated. The MPO activity in murine neutrophils was affected by Tyr and Ser/Thr dephosphorylation status. EPR studies identified a radiation-dependent generation of tyrosyl radical species in MPO and the radiation-induced tyrosyl radical generation was dose-dependent. In light of our previous findings that radiation-induces ACS in physiological solution (MPO-independent manner) [13], our current findings that radiation induces ACS generation by MPO-dependent manner implicate that γ-irradiation generates ACS by both MPO-independent and MPO-dependent pathways. LGM2605 has known radioprotecting and ACS scavenging properties and acts as an inhibitor of MPO [22], which make it a useful protective agent from radiation toxicity.

The residues that line the major active site cavity and have been shown to be phosphorylated *in vivo* are listed (Ser/S, Thr/T, Tyr/Y). The top of the table shows residues that are on the distal side of the heme and the bottom lists those on the proximal side. The first column uses common literature numbering (used throughout this manuscript), which does not account for the signal peptide and the first 166 residues in the nascent polypeptide. The Uniprot numbering column does account for these leader residues, which are not present in the coordinates shown in Figure 10 (PDB code 1DNW). The fifth column lists the location with respect to the active site heme (above, below, etc.) taken from the views show in Figure 10 B and 10C. The sixth column shows the per residue normalized solvent excluded surface area (SESA) and was calculated using the method of normalization described in the Materials & Methods. The final column provides comments on the location and specific roles of each candidate residue.

Supplementary Material

Refer to Web version on PubMed Central for supplementary material.

ACKNOWLEDGEMENTS AND FUNDING

This work was funded in part by: NIH-R01 CA133470 (MCS), NIH-1R21NS087406-01 (MCS), NIH-R03 CA180548 (MCS), 1P42ES023720-01 (MCS), the University of Pennsylvania Research Foundation (URF), and by pilot project support from 1P30 ES013508-02 awarded to MCS (its contents are solely the responsibility of the authors and do not necessarily represent the official views of the NIEHS, NIH). MA is manager of the Molecular Modeling Facility of Fox Chase Cancer Center, and this facility is supported in part by NIH grant P30 CA006927.

CONFLICTS OF INTEREST

Melpo Christofidou-Solomidou (MCS) reports grants from the National Institutes of Health (NIH) and the National Aeronautics and Space Administration (NASA) during the conduct of the study. In addition, MCS has patents No. US 10,045,951 B2, No. US 10,030,040 B2, and No. US 9,987,321 B2 issued and patents No. PCT/US2016/049780, No. PCT/US17/35960, and No. PCT/US2008/006694 pending, and has a founders equity position in LignaMed, LLC. MCS, AVP, and MA report grants from the NIH during the conduct of the study. RAP, W-TH, ENO, and OM have nothing to disclose.

ABBREVIATIONS

ABAH	4-aminobenzoic acid hydrazide, MPO inhibitor

Author Manuscript Author Manuscript Author Manuscript Author Manuscript

ACS	active chlorine species
ANOVA	analysis of variance
APF	3′-(p-aminophenyl) fluorescein
ClO^-	hypochlorite anion
DSP	dual specificity phosphatase
EPR	electron paramagnetic resonance
H_2O_2	hydrogen peroxide
hMPO	human myeloperoxidase
HOCl	hypochlorous acid
LGM2605	synthetic SDG
LPS	lipopolysaccharide
mMPO	murine myeloperoxidase
MPO	myeloperoxidase
•OH	hydroxyl radical
PBS	phosphate-buffered saline
PMN	polymorphonuclear neutrophils
PSTP	protein serine/threonine phosphatase
PTP	protein tyrosine phosphatase
RPM	revolutions per minute
RFU	relative fluorescence units
ROS	reactive oxygen species
SDG	secoisolariciresinol diglucoside
SEM	standard error of the mean
SESA	solvent excluded surface area
SOV	sodium orthovanadate, PTP inhibitor

REFERENCES

[1]. Lahtz C, Bates SE, Jiang Y, Li AX, Wu X, Hahn MA, Pfeifer GP, Gamma irradiation does not induce detectable changes in DNA methylation directly following exposure of human cells, PloS One, 7 (2012) e44858. [PubMed: 23024770]

[2]. Feldberg RS, Carew JA, Water radiolysis products and nucleotide damage in γ-irradiated DNA, Int J Radiat Biol Relat Stud Phys Chem Med, 40 (1981) 11–17. [PubMed: 6266972]

Author Manuscript Author Manuscript Author Manuscript Author Manuscript

[3]. Kuipers GK, Lafleur MVM, Characterization of DNA damage induced by gamma-radiation-derived water radicals, using DNA repair enzymes, Int J Radiat Biol, 74 (1998) 511–519. [PubMed: 9798962]

[4]. Cadet J, Douki T, Ravanat J-L, Oxidatively generated base damage to cellular DNA, Free Radical Biol Med, 49 (2010) 9–21. [PubMed: 20363317]

[5]. Spotheim-Maurizot M, Davidkova M, Radiation damage to DNA in DNA-protein complexes, Mutat Res, 711 (2011) 41–48. [PubMed: 21329707]

[6]. Saran M, Bertram H, Bors W, Czapski G, On the cytotoxicity of irradiated media. To what extent are stable products of radical chain reactions in physiological saline responsible for cell death?, Int J Radiat Biol, 64 (1993) 311–318. [PubMed: 8105009]

[7]. Saran M, Bors W, Radiation chemistry of physiological saline reinvestigated: evidence that chloride-derived intermediates play a key role in cytotoxicity, Radiat Res, 147 (1997) 70–77. [PubMed: 8989372]

[8]. Krokosz A, Komorowska MA, Szweda-Lewandowska Z, Radiation damage to human erythrocytes. Relative contribution of hydroxyl and chloride radicals in N2O-saturated buffers, Radiat Phys Chem, 77 (2008) 775–780.

[9]. Kudryasheva NS, Rozhko TV, Effect of low-dose ionizing radiation on luminous marine bacteria: radiation hormesis and toxicity, J Environ Radioact, 142 (2015) 68–77. [PubMed: 25644753]

[10]. Jeitner T, Lawrence D, Pulmonary autoimmunity and inflammation, in: Cohen MD, Zelikoff JT, Schlesinger RB (Eds.) Pulmonary Immunotoxicology, Kluwer Academic Publishers, Place Published, 2000, pp. 153–179.

[11]. De Ruysscher D, Niedermann G, Burnet NG, Siva S, Lee AWM, Hegi-Johnson F, Radiotherapy toxicity, Nat Rev Dis Primers, 5 (2019) 13. [PubMed: 30792503]

[12]. Kim JH, Jenrow KA, Brown SL, Mechanisms of radiation-induced normal tissue toxicity and implications for future clinical trials, Radiat Oncol J, 32 (2014) 103–115. [PubMed: 25324981]

[13]. Mishra OP, Popov AV, Pietrofesa RA, Christofidou-Solomidou M, Gamma-irradiation produces active chlorine species (ACS) in physiological solutions: Secoisolariciresinol diglucoside (SDG) scavenges ACS - A novel mechanism of DNA radioprotection, Biochim Biophys Acta, 1860 (2016) 1884–1897. [PubMed: 27261092]

[14]. Nauseef WM, Myeloperoxidase in human neutrophil host defence, Cell Microbiol, 16 (2014) 1146–1155. [PubMed: 24844117]

[15]. Malle E, Furtmuller PG, Sattler W, Obinger C, Myeloperoxidase: a target for new drug development?, Br J Pharmacol, 152 (2007) 838–854. [PubMed: 17592500]

[16]. Lazarevic-Pasti T, Leskovac A, Vasic V, Myeloperoxidase Inhibitors as Potential Drugs, Curr Drug Metab, 16 (2015) 168–190. [PubMed: 26279325]

[17]. Nussbaum C, Klinke A, Adam M, Baldus S, Sperandio M, Myeloperoxidase: a leukocyte-derived protagonist of inflammation and cardiovascular disease, Antioxid Redox Signal, 18 (2013) 692–713. [PubMed: 22823200]

[18]. Davies MJ, Myeloperoxidase-derived oxidation: mechanisms of biological damage and its prevention, J Clin Biochem Nutr, 48 (2011) 8–19. [PubMed: 21297906]

[19]. Pattison DI, Davies MJ, Hawkins CL, Reactions and reactivity of myeloperoxidase-derived oxidants: differential biological effects of hypochlorous and hypothiocyanous acids, Free Radic Res, 46 (2012) 975–995. [PubMed: 22348603]

[20]. Mishra OP, Simmons Nicholas, Sonia Tyagi, Ralph Pietrofesa, Shuvaev Vladimir V., Philipp Heretsch, Nicolaou KC and Melpo Christofidou-Solomidou, Synthesis and antioxidant evaluation of (S,S)- and (R,R)-secoisolariciresinol diglucosides (SDGs), Bioorg Med Chem Lett, (19) (2013) 5325–5328. [PubMed: 23978651]

[21]. Mishra OP, Pietrofesa R, Christofidou-Solomidou M, Novel synthetic (S,S) and (R,R)-secoisolariciresinol diglucosides (SDGs) protect naked plasmid and genomic DNA From gamma radiation damage, Radiat Res, 182 (2014) 102–110. [PubMed: 24945894]

[22]. Mishra OP, Popov AV, Pietrofesa RA, Nakamaru-Ogiso E, Andrake M, Christofidou-Solomidou M, Synthetic secoisolariciresinol diglucoside (LGM2605) inhibits myeloperoxidase activity in inflammatory cells, Biochim Biophys Acta Gen Subj, 1862 (2018) 1364–1375. [PubMed: 29524540]

Author Manuscript Author Manuscript Author Manuscript Author Manuscript

[23]. Ohnishi ST, Shinzawa-Itoh K, Ohta K, Yoshikawa S, Ohnishi T, New insights into the superoxide generation sites in bovine heart NADH-ubiquinone oxidoreductase (Complex I): the significance of protein-associated ubiquinone and the dynamic shifting of generation sites between semiflavin and semiquinone radicals, Biochim Biophys Acta, 1797 (2010) 1901–1909. [PubMed: 20513438]

[24]. Xu Y, Wang S, Hu Q, Gao S, Ma X, Zhang W, Shen Y, Chen F, Lai L, Pei J, CavityPlus: a web server for protein cavity detection with pharmacophore modelling, allosteric site identification and covalent ligand binding ability prediction, Nucleic Acids Res, 46 (2018) W374–W379. [PubMed: 29750256]

[25]. Bendell CJ, Liu S, Aumentado-Armstrong T, Istrate B, Cernek PT, Khan S, Picioreanu S, Zhao M, Murgita RA, Transient protein-protein interface prediction: datasets, features, algorithms, and the RAD-T predictor, BMC Bioinformatics, 15 (2014) 82. [PubMed: 24661439]

[26]. Pettersen EF, Goddard TD, Huang CC, Couch GS, Greenblatt DM, Meng EC, Ferrin TE, UCSF Chimera--a visualization system for exploratory research and analysis, J Comput Chem, 25 (2004) 1605–1612. [PubMed: 15264254]

[27]. Mishra OP, Popov AV, Pietrofesa RA, Nakamaru-Ogiso E, Andrake M, Christofidou-Solomidou M, Synthetic secoisolariciresinol diglucoside (LGM2605) inhibits myeloperoxidase activity in inflammatory cells, Biochim Biophys Acta Gen Subj, 1862 (2018) 1364–1375. [PubMed: 29524540]

[28]. Lee JC, Krochak R, Blouin A, Kanterakis S, Chatterjee S, Arguiri E, Vachani A, Solomides CC, Cengel KA, Christofidou-Solomidou M, Dietary flaxseed prevents radiation-induced oxidative lung damage, inflammation and fibrosis in a mouse model of thoracic radiation injury, Cancer Biol Ther, 8 (2009) 47–53. [PubMed: 18981722]

[29]. Christofidou-Solomidou M, Tyagi S, Tan KS, Hagan S, Pietrofesa R, Dukes F, Arguiri E, Heitjan DF, Solomides CC, Cengel KA, Dietary flaxseed administered post thoracic radiation treatment improves survival and mitigates radiation-induced pneumonopathy in mice, BMC Cancer, 11 (2011) 269. [PubMed: 21702963]

[30]. Christofidou-Solomidou M, Tyagi S, Pietrofesa R, Dukes F, Arguiri E, Turowski J, Grieshaber PA, Solomides CC, Cengel KA, Radioprotective role in lung of the flaxseed lignan complex enriched in the phenolic secoisolariciresinol diglucoside (SDG), Radiat Res, 178 (2012) 568–580. [PubMed: 23106213]

[31]. Pietrofesa R, Turowski J, Tyagi S, Dukes F, Arguiri E, Busch TM, Gallagher-Colombo SM, Solomides CC, Cengel KA, Christofidou-Solomidou M, Radiation mitigating properties of the lignan component in flaxseed, BMC Cancer, 13 (2013) 179. [PubMed: 23557217]

[32]. Klebanoff SJ, Myeloperoxidase: friend and foe, J Leukoc Biol, 77 (2005) 598–625. [PubMed: 15689384]

[33]. Bernofsky C, Nucleotide chloramines and neutrophil-mediated cytotoxicity, FASEB J, 5 (1991) 295–300. [PubMed: 1848195]

[34]. Bernofsky C, Bandara BMR, Hinojosa O, Strauss SL, Hypochlorite-modified adenine nucleotides: structure, spin-trapping, and formation by activated guinea pig polymorphonuclear leukocytes, Free Radical Res. Commun, 9 (1990) 303–315. [PubMed: 2167269]

[35]. Henderson JP, Byun J, Heinecke JW, Chlorination of nucleobases RNA and DNA by myeloperoxidase: a pathway for cytotoxicity and mutagenesis by activated phagocytes, Redox Rep, 4 (1999) 319–320. [PubMed: 10772075]

[36]. Ndrepepa G, Myeloperoxidase - A bridge linking inflammation and oxidative stress with cardiovascular disease, Clin Chim Acta, 493 (2019) 36–51. [PubMed: 30797769]

[37]. Khan AA, Alsahli MA, Rahmani AH, Myeloperoxidase as an Active Disease Biomarker: Recent Biochemical and Pathological Perspectives, Med Sci (Basel), 6 (2018).

[38]. Chami B, Martin NJJ, Dennis JM, Witting PK, Myeloperoxidase in the inflamed colon: A novel target for treating inflammatory bowel disease, Arch Biochem Biophys, 645 (2018) 61–71. [PubMed: 29548776]

[39]. Strzepa A, Pritchard KA, Dittel BN, Myeloperoxidase: A new player in autoimmunity, Cell Immunol, 317 (2017) 1–8. [PubMed: 28511921]

Author Manuscript Author Manuscript Author Manuscript Author Manuscript

[40]. Furtmuller PG, Zederbauer M, Jantschko W, Helm J, Bogner M, Jakopitsch C, Obinger C, Active site structure and catalytic mechanisms of human peroxidases, Arch Biochem Biophys, 445 (2006) 199–213. [PubMed: 16288970]

[41]. Marquez LA, Dunford HB, Kinetics of oxidation of tyrosine and dityrosine by myeloperoxidase compounds I and II. Implications for lipoprotein peroxidation studies, J Biol Chem, 270 (1995) 30434–30440. [PubMed: 8530471]

[42]. Heinecke JW, Tyrosyl radical production by myeloperoxidase: a phagocyte pathway for lipid peroxidation and dityrosine cross-linking of proteins, Toxicology, 177 (2002) 11–22. [PubMed: 12126792]

[43]. Arnhold J, Flemmig J, Human myeloperoxidase in innate and acquired immunity, Arch Biochem Biophys, 500 (2010) 92–106. [PubMed: 20399194]

[44]. Lardinois OM, Ortiz de Montellano PR, EPR spin-trapping of a myeloperoxidase protein radical, Biochem Biophys Res Commun, 270 (2000) 199–202. [PubMed: 10733927]

[45]. Heinecke JW, Oxidized amino acids: culprits in human atherosclerosis and indicators of oxidative stress, Free Radic Biol Med, 32 (2002) 1090–1101. [PubMed: 12031894]

[46]. Bayden AS, Yakovlev VA, Graves PR, Mikkelsen RB, Kellogg GE, Factors influencing protein tyrosine nitration--structure-based predictive models, Free Radic Biol Med, 50 (2011) 749–762. [PubMed: 21172423]

[47]. Reisz JA, Bansal N, Qian J, Zhao W, Furdui CM, Effects of ionizing radiation on biological molecules--mechanisms of damage and emerging methods of detection, Antioxid Redox Signal, 21 (2014) 260–292. [PubMed: 24382094]

[48]. Labbe DP, Hardy S, Tremblay ML, Protein tyrosine phosphatases in cancer: friends and foes!, Prog Mol Biol Transl Sci, 106 (2012) 253–306. [PubMed: 22340721]

[49]. Hunter T, Tyrosine phosphorylation: thirty years and counting, Curr Opin Cell Biol, 21 (2009) 140–146. [PubMed: 19269802]

[50]. Li J, Yen C, Liaw D, Podsypanina K, Bose S, Wang SI, Puc J, Miliaresis C, Rodgers L, McCombie R, Bigner SH, Giovanella BC, Ittmann M, Tycko B, Hibshoosh H, Wigler MH, Parsons R, PTEN, a putative protein tyrosine phosphatase gene mutated in human brain, breast, and prostate cancer, Science, 275 (1997) 1943–1947. [PubMed: 9072974]

[51]. Steck PA, Pershouse MA, Jasser SA, Yung WK, Lin H, Ligon AH, Langford LA, Baumgard ML, Hattier T, Davis T, Frye C, Hu R, Swedlund B, Teng DH, Tavtigian SV, Identification of a candidate tumour suppressor gene, MMAC1, at chromosome 10q23.3 that is mutated in multiple advanced cancers, Nat Genet, 15 (1997) 356–362. [PubMed: 9090379]

[52]. Salmena L, Carracedo A, Pandolfi PP, Tenets of PTEN tumor suppression, Cell, 133 (2008) 403–414. [PubMed: 18455982]

[53]. Tonks NK, Diltz CD, Fischer EH, Characterization of the major protein-tyrosine-phosphatases of human placenta, J Biol Chem, 263 (1988) 6731–6737. [PubMed: 2834387]

[54]. Barford D, Flint AJ, Tonks NK, Crystal structure of human protein tyrosine phosphatase 1B, Science, 263 (1994) 1397–1404. [PubMed: 8128219]

[55]. Camps M, Nichols A, Arkinstall S, Dual specificity phosphatases: a gene family for control of MAP kinase function, FASEB J, 14 (2000) 6–16. [PubMed: 10627275]

[56]. Storkey C, Davies MJ, Pattison DI, Reevaluation of the rate constants for the reaction of hypochlorous acid (HOCl) with cysteine, methionine, and peptide derivatives using a new competition kinetic approach, Free Radic Biol Med, 73 (2014) 60–66. [PubMed: 24794410]

[57]. Hornbeck PV, Zhang B, Murray B, Kornhauser JM, Latham V, Skrzypek E, PhosphoSitePlus, 2014: mutations, PTMs and recalibrations, Nucleic Acids Res, 43 (2015) D512–520. [PubMed: 25514926]

[58]. Kettle AJ, Winterbourn CC, Myeloperoxidase: Structure and Function of the Green Heme Peroxidase of Neutrophils, Heme Peroxidases, RSC Metallobiology Series4, (2015) pp. 272–308.

[59]. Issad T, Boute N, Boubekeur S, Lacasa D, Interaction of PTPB with the insulin receptor precursor during its biosynthesis in the endoplasmic reticulum, Biochimie, 87 (2005) 111–116. [PubMed: 15733745]

Author Manuscript Author Manuscript Author Manuscript Author Manuscript

[60]. Carpena X, Vidossich P, Schroettner K, Calisto BM, Banerjee S, Stampler J, Soudi M, Furtmuller PG, Rovira C, Fita I, Obinger C, Essential role of proximal histidine-asparagine interaction in mammalian peroxidases, J Biol Chem, 284 (2009) 25929–25937. [PubMed: 19608745]

Author Manuscript Author Manuscript Author Manuscript Author Manuscript

HIGHLIGHTS

- LGM2605 inhibits radiation-induced MPO-dependent ACS generation in MPO and neutrophils.
- Radiation-induced ACS generation is, in part, mediated by Tyr and Ser/Thr dephosphorylation.
- In non-irradiated cells, MPO activity is dependent on Tyr and Ser/Thr dephosphorylation.
- Dephosphorylation is a novel mechanism of radiation-induced MPO-mediated ACS generation.
- LGM2605 is a promising potential attenuator of radiation-induced chlorination damage.

Author Manuscript Author Manuscript Author Manuscript Author Manuscript

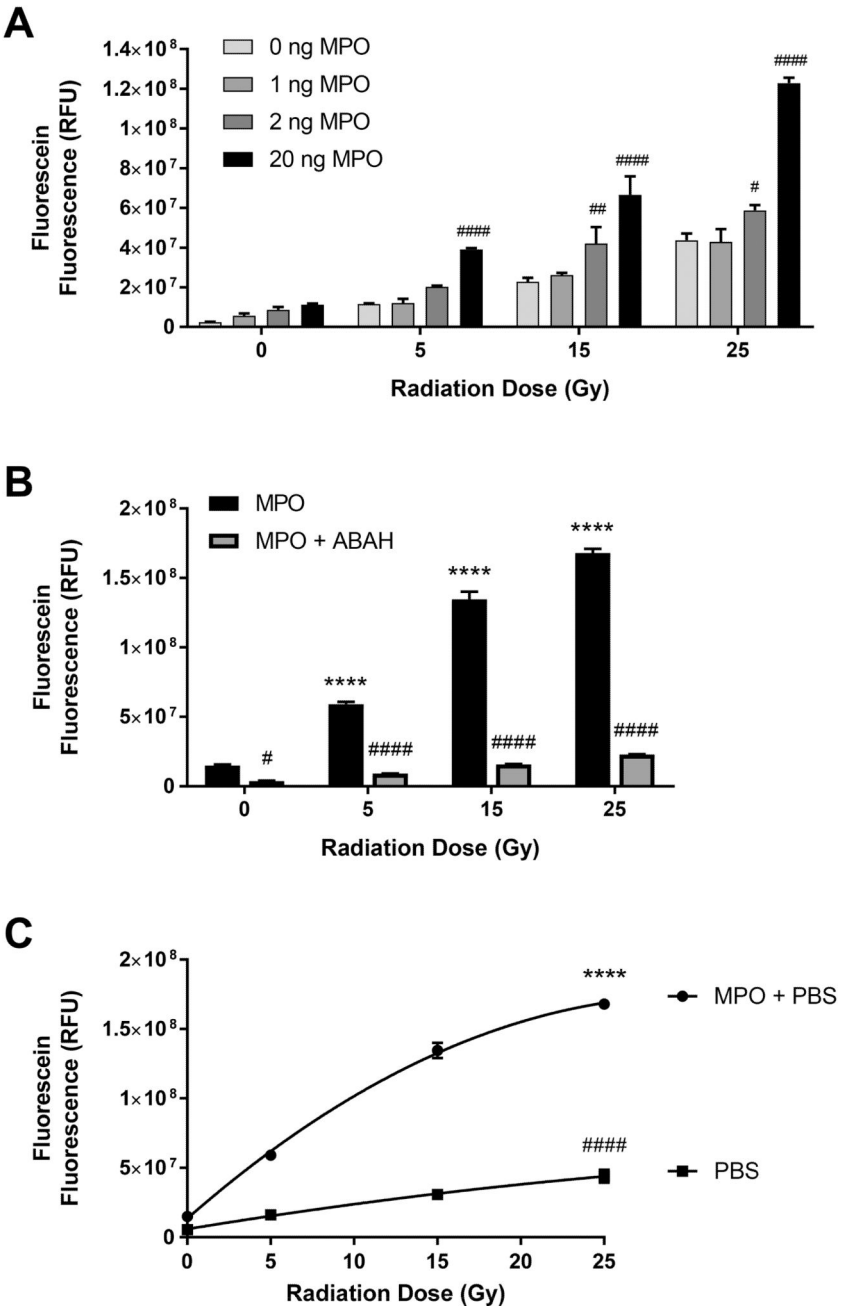

Figure 1: γ-Radiation Induces MPO-dependent Generation of ACS

Figure 1A shows the effect of various doses of γ-radiation ranging from 0–25 Gy on ACS generation using different concentrations (1–20 ng/well) of MPO. Figure 1B shows the MPO activity-dependence of radiation-induced ACS generation using MPO inhibitor ABAH (100 μM) and MPO (20 ng/200 μl medium/well). Figure 1C shows the kinetic pattern of radiation-induced MPO-dependent and MPO-independent ACS generation as a function of radiation dose. Asterisks shown in figures indicate statistically significant differences from 0 Gy (**** : $p < 0.0001$), while # shown in figures indicate statistically significant differences

from 0 ng MPO (**A**), MPO (**B**), and MPO + PBS (**C**) (# : $p < 0.05$, ## : $p < 0.01$, and #### : $p < 0.001$).

Author Manuscript Author Manuscript Author Manuscript Author Manuscript

Author Manuscript Author Manuscript Author Manuscript Author Manuscript

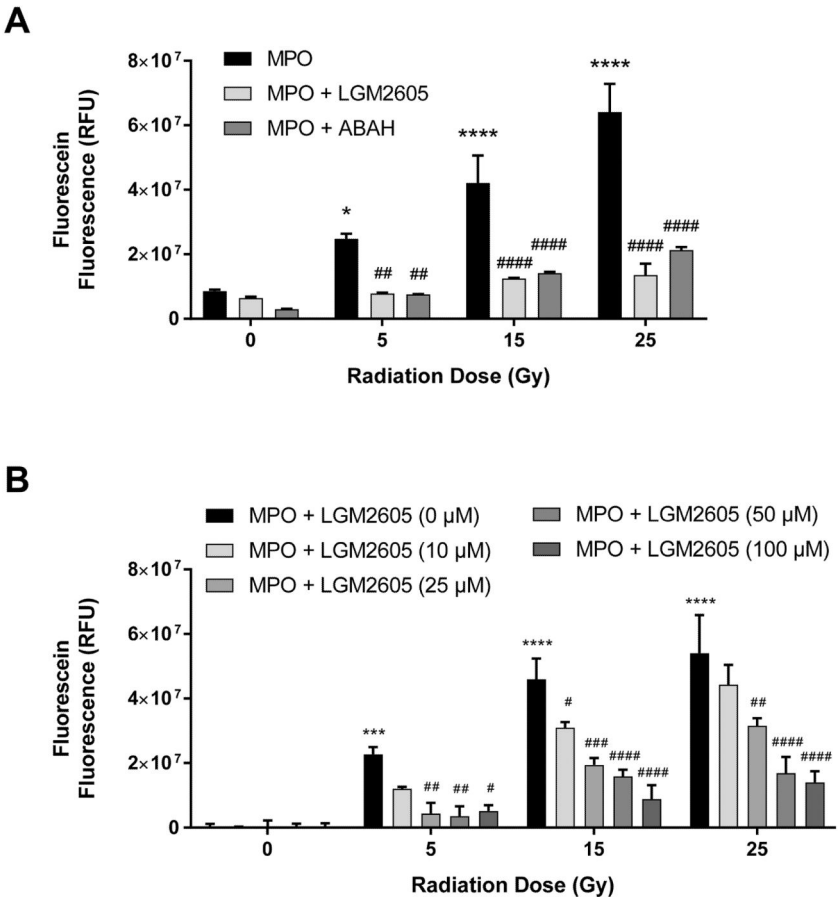

Figure 2: LGM2605 Decreases γ-Radiation-induced, MPO-dependent Generation of ACS, *In Vitro*

Figure 2A shows the effect of LGM2605 (100 μM) on radiation-induced, MPO-dependent generation of ACS in the presence of MPO inhibitor ABAH (100 μM). Figure 2B shows the effect of various doses of LGM2605 on radiation induced, MPO-dependent generation of ACS. Asterisks shown in figures indicate statistically significant differences from 0 Gy (* : $p < 0.05$, *** : $p < 0.001$, and **** : $p < 0.0001$), while # shown in figures indicate statistically significant differences from MPO (**A**) and MPO + LGM2605 (0 μM) (**B**) (# : $p < 0.05$, ## : $p < 0.01$, ### : $p < 0.005$, and #### : $p < 0.001$).

Author Manuscript Author Manuscript Author Manuscript Author Manuscript

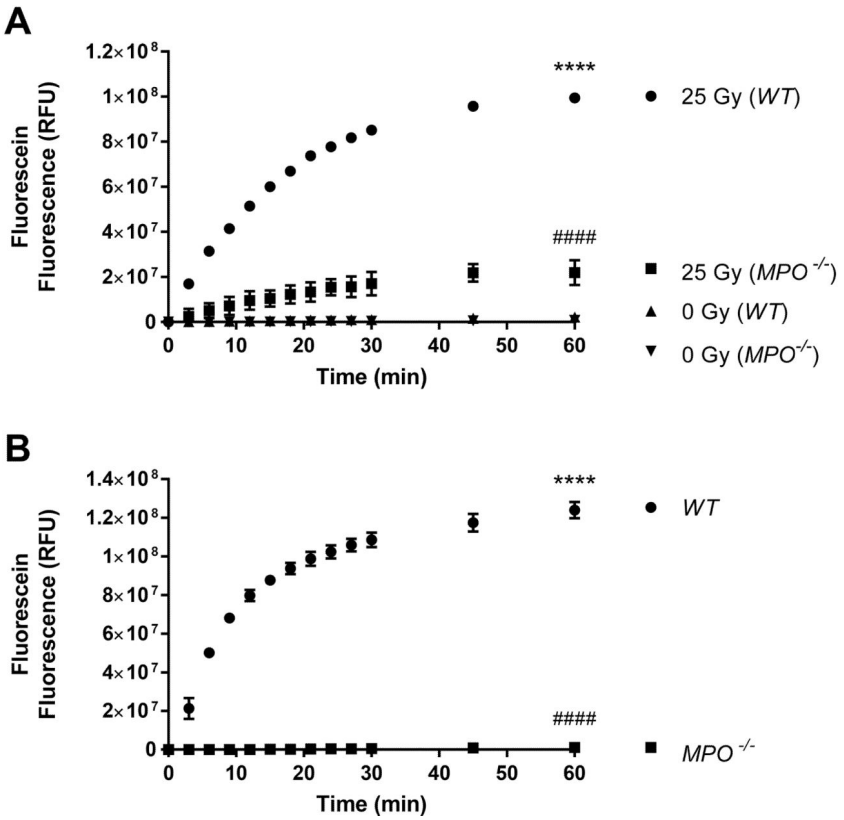

Figure 3: Radiation-induced, MPO-dependent Generation of ACS in Neutrophils from Wild Type and MPO Knockout Mice

Figure 3A shows the effect of γ-radiation on MPO-dependent ACS generation in elicited neutrophils from wild type and $MPO^{-/-}$ knockout mice in the presence of MPO inhibitor ABAH (100 μM). mMPO activity in elicited neutrophils from wild-type and MPO knockout mice is shown in Figure 3B. Asterisks shown in figures indicate statistically significant differences between treatment groups from 0 min (**** : $p < 0.0001$), while # shown in figures indicate statistically significant differences from 25 Gy (*WT*) (**A**) and WT (**B**) (#### : $p < 0.001$).

Author Manuscript Author Manuscript Author Manuscript Author Manuscript

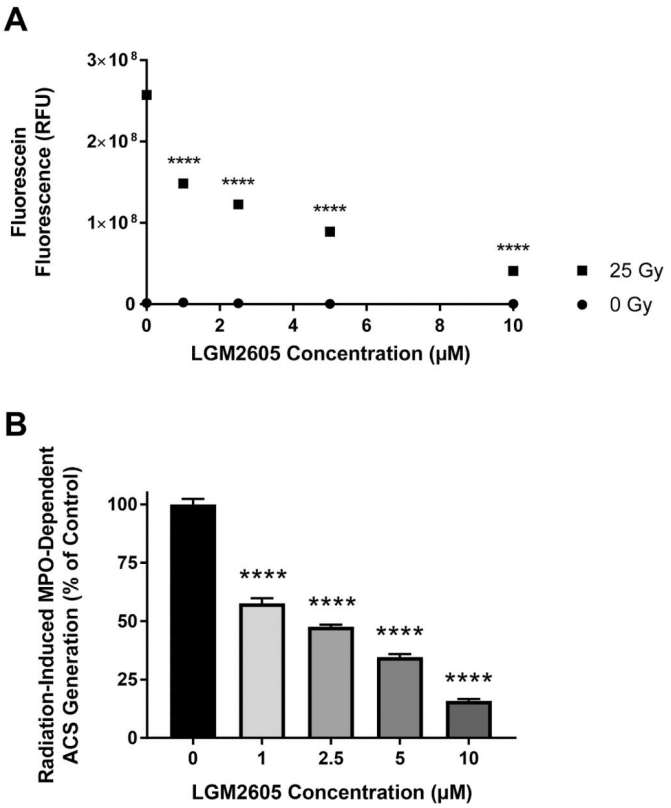

Figure 4: Radiation-induced, MPO-dependent Generation of ACS in Murine Neutrophils: Effect of LGM2605

Figures 4A and 4B show the effect of γ-radiation on MPO-dependent ACS generation in the presence of MPO inhibitor ABAH (100 μM) and the effect of LGM2605 in murine neutrophils. Figure 4B shows the effect of LGM2605 on MPO-dependent ACS generation as percent of control (value in the absence of LGM2605). Asterisks shown in figures indicate statistically significant differences between treatment groups from 0 μM LGM2605 (**** : $p < 0.0001$).

Author Manuscript Author Manuscript Author Manuscript Author Manuscript

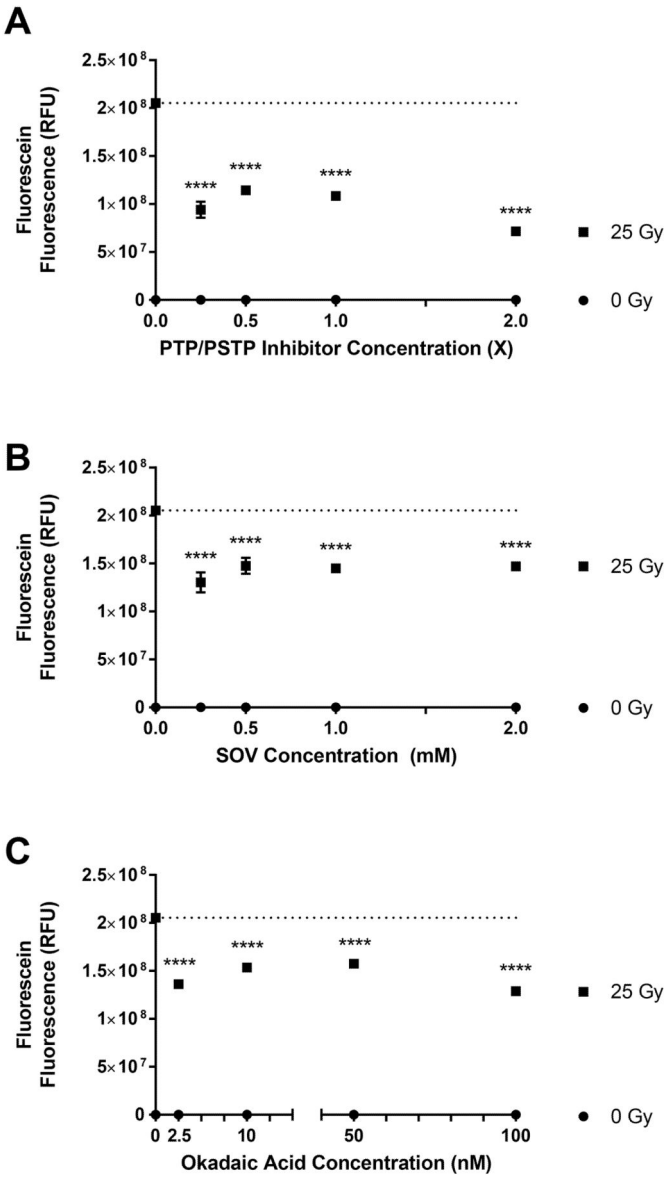

Author Manuscript Author Manuscript Author Manuscript Author Manuscript

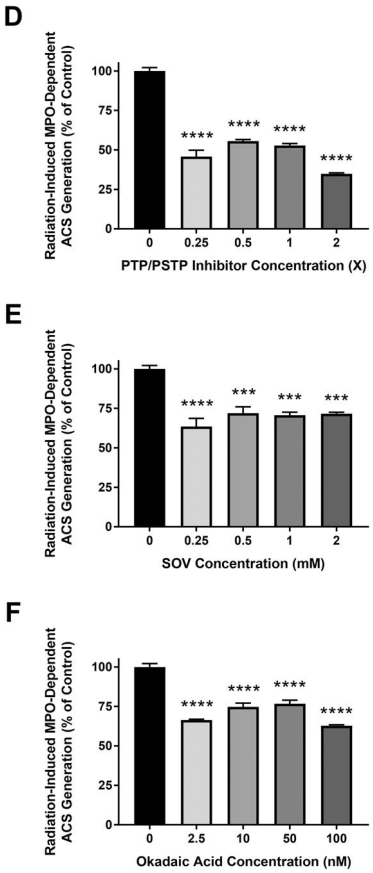

Figure 5: Radiation-induced, MPO-dependent Generation of ACS in Murine Neutrophils: Effect of Protein Phosphatase Inhibitors

Figures 5A, 5B, and 5C show the effect of γ-radiation on ACS generation in the presence of MPO inhibitor ABAH (100 μM) in murine neutrophils in the presence of: PTP+PSTP inhibitors, PTP inhibitor (SOV), and PSTP inhibitor (okadaic acid). The dotted line represents the mean fluorescein fluorescence level with 25 Gy exposure in the absence of any MPO inhibitor. Figures 5D, 5E, and 5F show the effect of protein phosphatase inhibitors as percent of control. Inhibitors were added prior to radiation exposure. Asterisks shown in figures indicate statistically significant differences from baseline, where no enzyme inhibitor was added (*** : $p < 0.001$ and **** : $p < 0.0001$).

Author Manuscript Author Manuscript Author Manuscript Author Manuscript

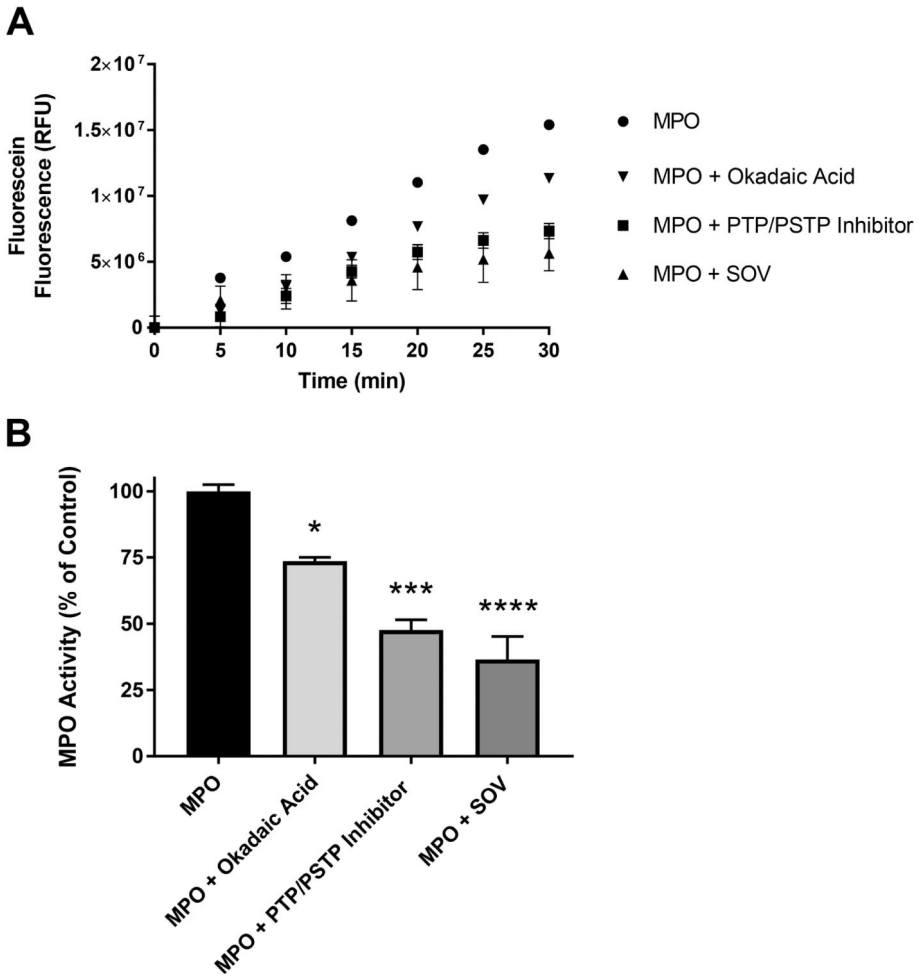

Figure 6: Dephosphorylation-Dependence of MPO Activity in Murine Neutrophils: Effect of Protein Phosphatase Inhibitors

Figure 6A show the effect of protein phosphatase inhibitors on MPO activity in murine neutrophils in the presence of PTP+PSTP inhibitors (0.25x), PTP inhibitor (SOV, 0.25 mM) and PSTP inhibitor (okadaic acid, 50 nM). Figures 6B shows the percent of MPO activity. Asterisks shown in figures indicate statistically significant differences from the MPO-only group (* : $p < 0.05$, *** : $p < 0.001$, and **** : $p < 0.0001$).

Author Manuscript Author Manuscript Author Manuscript Author Manuscript

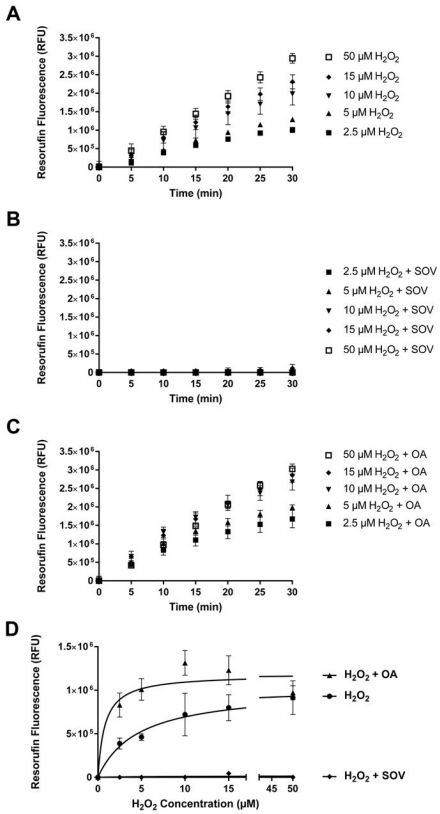

Figure 7: Dephosphorylation-Dependence of Peroxidase Cycle of MPO in Murine Neutrophils

Figure 7 shows the effect of protein phosphatase inhibitors on Peroxidase Cycle of MPO activity in murine neutrophil controls (Figure 7A), in the presence of PTP inhibitor, SOV (1.0 mM) (Figure 7B), in the presence of PSTP inhibitor, okadaic Acid (100 nM) (Figure 7C), and peroxidase cycle activity at various concentrations of H_2O_2 in the presence of protein phosphatase inhibitors (Figure 7D).

Author Manuscript Author Manuscript Author Manuscript Author Manuscript

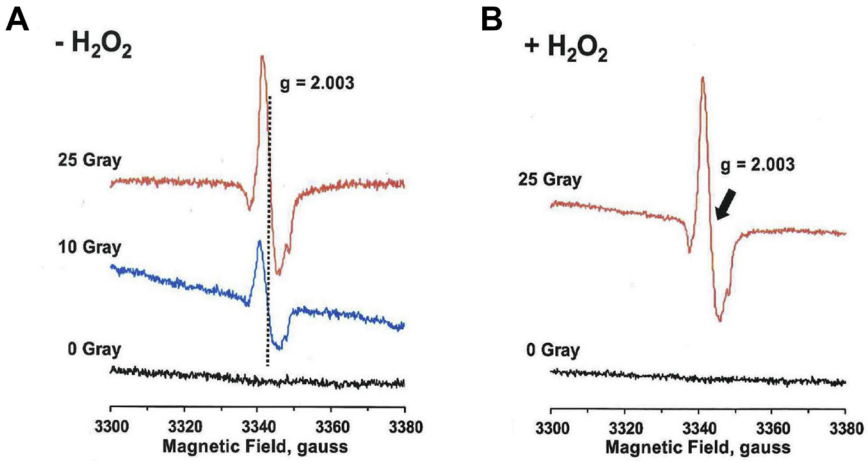

Figure 8: EPR Spectra of Radiation-induced Tyrosyl Radical Species in hMPO

Figure 8A shows the EPR spectra of hMPO for 0 Gy, 10 Gy, and 25 Gy radiation exposure. Figure 8B shows hMPO spectra for 0 Gy + H_2O_2 and 25 Gy + H_2O_2.

Author Manuscript Author Manuscript Author Manuscript Author Manuscript

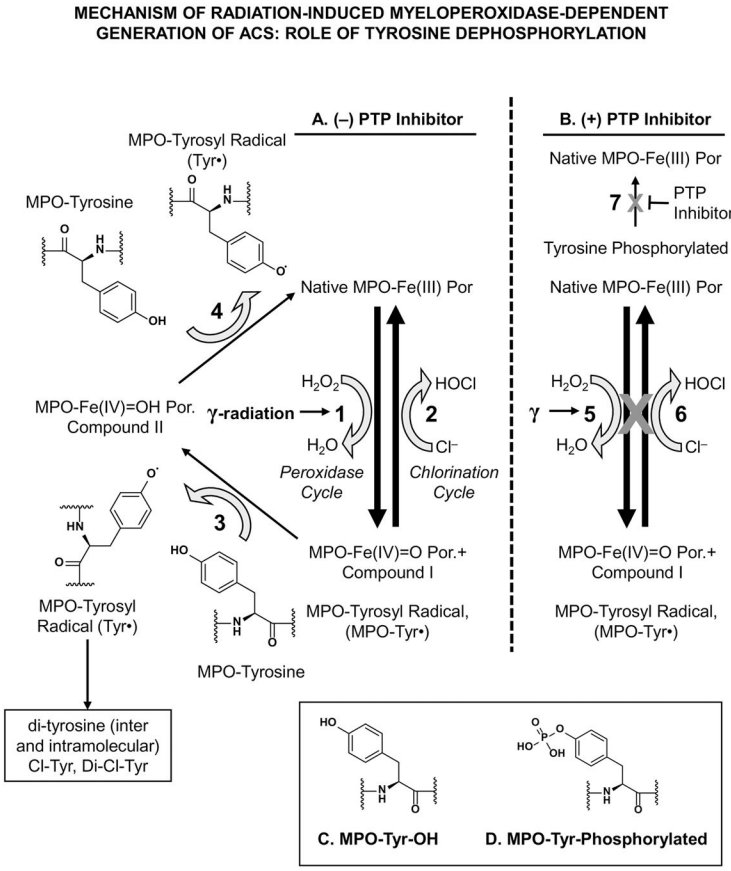

Figure 9: Proposed Mechanism of Radiation-induced, MPO-Dependent Generation of ACS: Role of Tyrosine Dephosphorylation

Figure 9 shows the proposed mechanism of radiation-induced, MPO-dependent ACS generation without protein tyrosine phosphatase (PTP) inhibitor (Figure 9A) and with PTP inhibitor (Figure 9B). Figures 9C and 9D show MPO-Tyr-OH and MPO-Tyr-phosphorylated structures.

Author Manuscript Author Manuscript Author Manuscript Author Manuscript

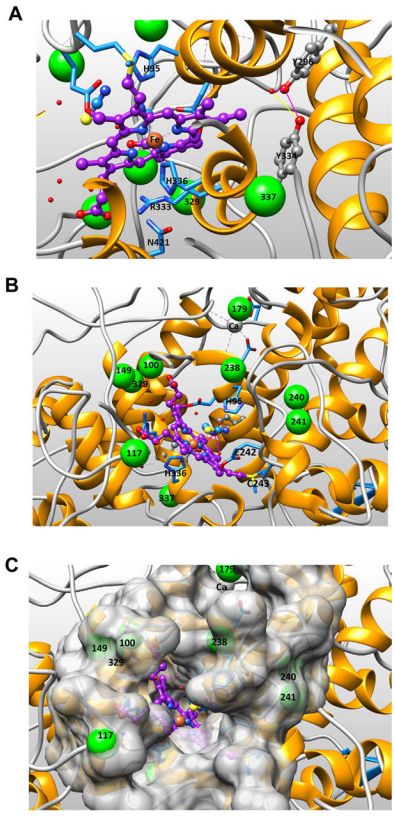

Figure 10: Proximal and Distal Sides of the Active Site Cavity of Myeloperoxidase

Figure 10A shows the proximal side of the active site of hMPO (PDB code 1DNW). The proximal triad amino acids His336, Arg333 and Asn421 are shown directly underneath the heme portrayed in purple ball-and-stick representation. Nearby in gray ball-and-stick representation are Tyr334 and Tyr296, and their potential hydrogen bonding interaction (dephosphorylated form) is shown. Green spheres mark the position of Ser/Thr residues (enlarged -OH position) labeled with corresponding residue number according to literature numbering (see Table 1). Figure 10B shows the distal side of MPO active site cavity. The two residues liganding the heme iron, His95 and His336, are shown as sticks, as well as cyanide and thiocyanate ligands shown in yellow and blue ball-and-stick just above the heme iron. Heme (purple), Fe (orange), Tyr (gray ball-and-sticks) and Ser/Thr residues (large green spheres). Figure 10C shows the distal side of the active site cavity from the same angle as Figure 10B but adding the surface representation of the cavity to view the relative placement of residues in the active site with respect to the buried heme catalytic center.

Author Manuscript

Author Manuscript

Author Manuscript

Author Manuscript

Table 1:

Residues in the Major Active Site Cavity that Could Be Phosphorylated

Lit No.	Uniprot No.	Known Phosphosite	Side of Heme	Near Active Site	Surface Access	Comments
T100	T266	Yes	Distal	Yes	0.82	Very close to Heme propionate group
T117	T283	Yes	Distal	At top opening	0.79	Phosphorylation unlikely to sterically block distal cavity, but could repel negatively charged substrates
S149	S315	Yes	Distal	Yes	0.42	Distal cavity candidate; hydrogen bonds to R424 that in turn hydrogen bonds to Heme COOH
S179	S345	Yes	Distal	No	0.63	Near Ca^{2+} binding site
T238	T404	Yes	Distal	Yes	1.05	Distal candidate; hydrogen bonds to H95 and R239; phosphorylation would directly block substrate access
S240	S406	Yes	Distal	Above	0.14	Perhaps important for positioning E242/C243 that covalently link Heme
S241	S407	Yes	Distal	Above	0.42	Perhaps important for positioning E242/C243 that covalently link Heme
Y296	Y462	Yes	Proximal	Below	0.54	Prime proximal side candidate, not accessible; phosphorylation could alter heme position
T329	T495	Yes	Proximal	Below	0.80	Back wall of the active site; phosphorylation could distort active site
Y334	Y500	Yes	Proximal	Below	0.31	Prime proximal side candidate; phosphorylation could affect active site heme configuration and redox chemistry
S337	S503	Yes	Proximal	Below	0.21	Proximal deep part of cavity